Electronic structures of the $YBa_2Cu_3O_{7-x}$ surface and its modification by sputtering and adatoms of Ti and Cu

H. M. Meyer III, D. M. Hill, T. J. Wagener, Y. Gao, and J. H. Weaver
Department of Chemical Engineering and Materials Science, University of Minnesota, Minneapolis, Minnesota 55455

D. W. Capone II and K. C. Goretta
Materials Science Division, Building 223, Argonne National Laboratory, Argonne, Illinois 60439
(Received 29 February 1988)

We present x-ray and inverse photoemission results for fractured surfaces of $YBa_2Cu_3O_{6.9}$ before and after surface modification by Ar ion bombardment and the deposition of adatoms of Ti and Cu. Representative results are compared for samples prepared in three different ways. Two of the sample types exhibit substantial emission from grain-boundary phases because of both intergranular and transgranular fracture; they produce results that are very similar to those presented thus far in the literature. A third type was nearly free of contamination and clearly showed spectral features characteristic of the superconductor. Comparison of these nearly contamination-free valence-band results to those for clean $La_{1.85}Sr_{0.15}CuO_4$ shows remarkably similar x-ray photoemission spectroscopy densities of states, with subtle differences near the Fermi level and at 3 eV. Inverse photoemission results show the top of the Cu-O hybrid orbitals to be 2 eV above E_F and the empty states of Y and Ba at higher energy. Comparison with one-electron densities of states shows reasonable agreement, but there are large differences within the set of calculated results, and it is unclear from the valence bands alone how to account for final-state Cu *d-d* Coulomb correlation effects (satellite features show these effects very clearly). Argon sputtering for both types of samples shows destruction of the superconductor, with differences that can be related to sample surface quality. The deposition of adatoms of Ti and Cu results in reaction associated with oxygen withdrawal from the near-surface region. Studies of the Cu $2p_{3/2}$ line shape show that the deposition of as little as ~ 1 monolayer equivalent of Ti or Cu reduces the formal Cu^{2+} emission within the probed volume (30–50 Å deep). Core-level analysis shows that this chemical reduction of Cu is accompanied by crystal-structure modifications as well. Studies of Cu adatom interactions reveal the progression from Cu^{2+} to Cu^{1+} and, ultimately, to Cu metal as the overlayer thickens (Cu $2p_{3/2}$ binding energy 932.5 eV for Cu metal, 933.1 eV for Ci^{1+}, and 932.8 eV for the superconductor). Valence-band results during interface formation show the disappearance of emission near the Fermi level, consistent with the loss of Cu^{2+}-O covalent bonds of the superconductor.

I. INTRODUCTION

The discovery of copper-oxide-based materials[1] with superconducting transition temperatures above 90 K has resulted in a surge of scientific inquiry. Many efforts have sought to isolate the fundmental characteristics responsible for superconductivity. The various forms of electron spectroscopy have contributed to these efforts by revealing the electronic states on either side of the Fermi level, E_F.[2–21] For the 2:1:4-based superconductors, early attempts at synthesis produced samples which were largely free of carbon and grain-boundary phases, as judged by photoemission studies of fractured bulk samples.[19] However, the synthesis of the 1:2:3-based superconductors of the form $YBa_2Cu_3O_{7-x}$ produced samples which exhibited significant amounts of Ba-containing contamination, again as judged from photoemission results for fractured samples.[19] This has made it difficult to identify the valence-band and core-level signatures of the basic superconducting phase. Indeed, there have been many interesting discussions about spectral features which have ultimately fallen by the wayside as sample synthesis has improved.

In this paper, we present x-ray photoemission results for samples of $YBa_2Cu_3O_{6.9}$ that were fractured *in situ* in ultrahigh vacuum. Valence-band and core-level data from three representative samples make it possible to identify the spectral signatures of the clean 1:2:3 superconductor and the contributions from contamination. With these results, we have compared the x-ray photoemission spectroscopy (XPS) results for the 1:2:3 superconductor to those for the 2:1:4 $La_{1.85}Sr_{0.15}CuO_4$ system, finding remarkably similar overall densities of states (spectral features, bandwidths). Indeed, the similarities appear to be greater than might have been expected from the one-electron band calculations.[22–27] Inverse photoemission results show the top of the Cu-O hybrid states and the empty Y and Ba *d* bands, as well as the relatively sharp Ba 4*f* levels. These results facilitate comparisons with the calculations, but the diversity of theoretical results complicates a simple comparison which would make it possible to determine final-state effects, although such effects are known to be significant based on analysis of the Cu satellite structures.[15,16,23,28]

Since one of the important issues for these materials involves their surface stability, we have examined the changes in the electronic states induced by Ar^+ ion sputtering and metal adatom deposition. Our results show that the electronic properties of the superconductor are adversely modified by sputtering because of structural changes. Studies of the interactions of Ti and Cu adatoms with both types of $YBa_2Cu_3O_{6.9}$ show severe modification of the properties of the surface region. These can be understood in terms of the removal of oxygen from the superconductor and the formation of metal oxides. Such interactions are not limited to the withdrawal of oxygen from the superconductor chains but rather are associated with substantial substrate disruption. As a result, the metal/superconductor interface should be thought of as a complex region with a metal overlayer which ultimately appears when oxygen removal from the substrate becomes kinetically limited, a metal-oxide region in contact with the disrupted superconductor, and then a buried superconductor. Room-temperature depositions of Ti and Cu adatoms of less than a monolayer equivalent induce changes within the entire volume probed by photoemission (30–50 Å depth).

This paper is structured as follows. After a brief description of our experimental procedures and sample preparation techniques (Sec. II), we present core-level and valence-band results for three differently-prepared samples (Sec. III A). We compare these results to those for the 2:1:4 superconductors and to band calculations in Sec. III B. In Sec. III C we describe the results of surface modification by Ar ion sputtering and by the deposition of adatoms of Ti and Cu.

II. EXPERIMENTAL TECHNIQUE

X-ray photoemission studies were performed in an ultrahigh vacuum system consisting of an analysis chamber separated by a gate valve from a sample preparation chamber. In the analysis chamber, a monochromatized photon beam (Al $K\alpha$, $h\nu = 1486.6$ eV) was focused onto the sample surface and the emitted electrons were energy dispersed with a Surface Sciences Instruments hemispherical analyzer onto a position-sensitive detector. The size of the focused x-ray beam was 300 μm and the pass energy of the analyzer was 50 eV. A dedicated HP9836C computer was used for data acquisition and analysis. For the inverse photoemission measurements, a monochromatic electron beam was directed onto the sample at normal incidence and the distribution of emitted photons was measured with a monochromator and position sensitive detector. The size of the electron beam was approximately 1×5 mm and the overall resolution was 0.3–0.6 eV for photon energies 12–44 eV. Further experimental details can be found in Ref. 29.

The polycrystalline $YBa_2Cu_3O_{6.9}$ samples had densities varying from 71% to 95% and superconducting transition temperatures of ~ 92 K.[30] They were prepared from CuO, Y_2O_3, and $BaCO_3$ powders mixed to give the correct final stoichiometry. The preparation procedures differed in the initial grinding of the oxides. The powders for sample *A* were wet milled in a slurry of isopropyl alcohol using Zr_2O_3 milling balls and were subsequently heated in air at 950 °C. The milling and heating procedure was repeated three times. The final sintering process was performed in O_2 with a stepwise heating schedule, achieving a maximum temperature of 1035 °C after 12 h and returning to room temperature in an additional 19 h. The measured density of sample *A* was 93%. For sample *B*, a wet vibratory milling procedure in isopropyl alcohol was used. Heating in air to 950 °C was again done following three separate milling steps. The mixed oxide powder was subjected to the same heating schedule in O_2, and the final sample *B* had a measured density of 71%. Sample *C* was pressed into a bar from a fine mesh powder obtained from Rhone-Poulenc (France) and subjected to a heating schedule that reached 950 °C at its maximum. It had a density of $\sim 95\%$. (Rhone-Poulenc has not released the detailed stoichiometry and size distribution of the starting powders).

Fresh surfaces were prepared by fracturing sample posts *in situ* at pressures of $\sim 5 \times 10^{-11}$ Torr. All measurements were performed at room temperature. For the interface work, adatoms of titanium and copper were deposited onto freshly fractured $YBa_2Cu_3O_{6.9}$ surfaces according to standard sublimation or evaporation procedures. During deposition, the system pressure was always below 1×10^{-10} Torr. The sublimation of Ti produced chemically active chamber walls and led to measurement pressures of $\sim 6 \times 10^{-11}$ Torr. Coverages ranging from 0.25 to 90 Å for Ti and 0.5 to 86 Å for Cu were achieved by depositing the adatoms at rates of ~ 1 Å/min, as monitored by a quartz-crystal oscillator situated near the sample. The amount of deposited material is given in angstrom units. For Ti, it would take 3.53 Å to equal one monolayer of substrate atoms for the Cu-O (001) plane of the $YBa_2Cu_3O_{6.9}$ structure (planar density 2×10^{15} atoms/cm^2). For Cu, it would take 2.35 Å to equal one monolayer. It should be kept in mind that these adatoms induce reaction and that the amount of modified surface-plus-overlayer substantially exceeds the amount of material deposited, as we will show.

For the sputtering experiments, the samples were again prepared by fracturing *in situ*. Following surface characterization, we subjected the sample to bombardment with 500-eV Ar ions for predetermined amounts of time (typically 30 s) and then examined the effects with core-level photoemission. In this way, it was possible to follow changes at the surface for both the superconducting and grain-boundary phases.

In all of these XPS experiments, the energy distribution curves (EDC's) for the photoemitted electrons were measured for the valence bands and shallow core levels within 35 eV of the Fermi level and for the deeper O 1*s*, Cu $2p_{3/2}$, Ba $3d_{5/2}$, Y $3d_{3/2,5/2}$, and Ti $2p_{3/2}$ core levels. The region corresponding to the C 1*s* emission was also scanned to assess sample cleanliness and chemisorption from the vacuum system. These core-level spectra were fit with Gaussian functions following the subtraction of S-shaped backgrounds to obtain the binding-energy positions, integrated areas, and peak widths at each stage during surface modification or interface evolution. In the in-

verse photoemission experiments, we examined the empty electronic states to ~20 eV above E_F.

A. $YBa_2Cu_3O_{6.9}$ surfaces

In Fig. 1 we show the O 1*s* and Ba $3d_{5/2}$ core-level EDC's (central panel), the Cu $2p_{3/2}$ and Y $3d_{3/2,5/2}$ EDC's (top panel), and valence band and shallow corelevel EDC's (bottom panel) for freshly fractured samples of $YBa_2Cu_3O_{6.9}$. The letters *A*, *B*, and *C* given alongside the spectra identify the origin of the samples, as discussed above. For samples *A* and *B*, the O and Ba EDC's show multiple electronic states with large chemical shifts between the spectral maxima (~2.4 eV for O and ~1.6 eV for Ba $3d_{5/2}$). Comparison to the results for sample *C* indicates that the higher-binding-energy features are due to contamination. Presumably, this contamination is present in the grain boundaries of the bulk sample and is exposed by intergranular fracture; it has been a substantial component in all results in the literature, most of which resemble *A* or *B*.[18] For sample *C*, however, there is only a slight asymmetry in the Ba emission and a small shoulder for oxygen. We conclude that the amount of contamination is very small, although still not zero (see dashed line for O 1*s* emission). Comparison of the O 1*s* results for sample *C* to those for contamination-free $La_{1.85}Sr_{0.15}CuO_4$ shows that sample *C* had slightly more contamination.[20] We also note that the amount of impurity O 1*s* emission from sample *C* was cleave dependent, with different surfaces of the same sample showing variations in intensity (up to 25% of the total O 1*s* intensity and always much less than *A* or *B*). These results illustrate the difficulties in preparing single phase, contiguous samples with clean grain boundaries.

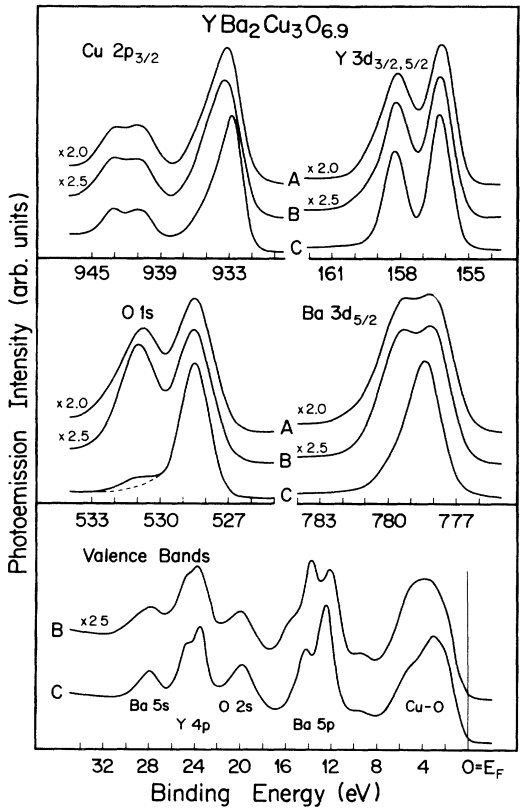

FIG. 1. Core-level and valence-band energy distribution curves (EDC's) for three different samples of $YBa_2Cu_3O_{6.9}$. Sample preparation differs only in the milling procedure used to form the starting powders. The results for samples *A* and *B*, which are similar to data presented by ourselves and others in the literature, exhibit substantial contributions from contamination exposed by *in situ* fracturing of bulk samples. The results for sample *C* are almost free of this grain-boundary contamination, as judged by the O 1*s* and Ba $3d_{5/2}$ line shape, the sharpening of the Cu $2p_{3/2}$ emission, and the better resolved shallow Y and Ba core emission. For states near the Fermi level, there is a significant change as the contribution from the second phase near 5 eV is reduced.

Aging *in situ* of both sample *C* and the contamination-free $La_{1.85}Sr_{0.15}CuO_4$ sample resulted in the growth of the O 1*s* shoulder because of chemisorption of residual H_2O, CO, or CO_2 in the vacuum system. Interestingly, the starting O 1*s* spectrum for sample *C* was nearly identical to that obtained for $La_{1.85}Sr_{0.15}CuO_4$ after the latter had been resident in the ultrahigh vacuum (UHV) chamber for 12 h [the equivalent of 2–3 L (1 L = one langmuir = 10^{-6} Torr sec) of total exposure].[20] No such time dependence was observed for samples *A* and *B*, presumably because such small changes would have been overwhelmed by the already-large contamination feature. In order to determine possible x-ray induced changes, we repetitively examined the O and Cu $2p_{3/2}$ core-level emission, acquiring data over a 24-h period. There were no changes that might be related to x-ray-induced loss of a 3^+ Cu configuration, as reported by Steiner *et al.*[17] for $NaCuO_2$. Finally, investigation of the C 1*s* spectra for samples *A* and *B* showed the presence of carbon, again consistent with intergranular fracture and exposure of residual carbonates. Estimates based on photoionization cross sections and the relative emission intensities suggest carbon to be present at the 10–15-at.% level in samples *A* and *B*. Sample *C* showed less than 1 at.% of carbon.

The results for the Ba $3d_{5/2}$ emission shown in Fig. 1 are as unequivocal as those for oxygen in pointing to multiple-bonding configurations. For samples *A* and *B*, the emission from the impurity phase was almost equal in intensity to that of the superconductor phase, shifted ~1.6 to higher binding energy. For sample *C*, there was a single structure at 778.3 eV that exhibited an asymmetry to higher binding energy. Exposure of these samples to the atmosphere greatly increases the emission from the high-binding-energy component, even for samples *A* and *B*. As Brundle and co-workers recently pointed out,[18] it is likely that the Ba contaminant emission is composed of more than one component, probably from a combination of Ba oxides, hydroxides, and carbonates.

From these results, we conclude that fracturing of sample *C* produced clean surfaces with a small amount of contamination due to regions of imperfection in the sample. Electron microscopy results for these same surfaces did reveal the presence of voids (6–15% of the visual image under 5000× magnification), but there was much more effective sintering of the grains and less intergranular

fracturing than for samples *A* or *B*. From the range of results for C, O, and Ba shown in the central panel of Fig. 1, it would seem reasonable that measurements which are sensitive to the surface (e.g., tunneling, photoemission, Auger spectroscopy, electron-energy-loss spectroscopy, inverse photoemission, photon-stimulated desorption, and others) will be much more reliable with these higher-quality samples (or with perfect single crystals).

At the top left-hand side of Fig. 1 we show Cu $2p_{3/2}$ core-level EDC's for samples *A*, *B*, and *C*. These have been normalized to constant height to emphasize changes in peak positions and line shape. For samples *A* and *B*, there is a main line near 933 eV and a doublet at higher binding energy. Comparison with published XPS results for other $YBa_2Cu_3O_{6.9}$ samples shows basically the same spectral appearance with a dominant feature near 933 eV and a broad doublet at higher energy.[17,18] For sample *C*, the main line maximum is shifted to lower binding energy by $\sim$0.5 eV and is sharper, but the satellite features are unchanged in position. For samples *A* and *B*, the integrated emission intensity for the satellites relative to the main peak is $\sim$35% higher than for sample *C*. Further, the satellite-to-main-line intensity ratio and the main-line binding energy for sample *C* compared favorably to results for our contamination-free $La_{1.85}Sr_{0.15}CuO_4$. We conclude that the grain-boundary phase present in samples *A* and *B* broadens the main Cu $2p_{3/2}$ line asymmetrically to higher binding energy and increases the satellite intensity. This indicates that Cu atoms responsible for these spectral changes have the same *nominal* valence, but the details of the final-state screening differ because of the bonding configurations (numbers, types, and distances for nearest neighbors and the details of the covalent bonds). Comparison of the Cu $2p$ core-level emission for these superconductors to that for single crystals of CuO doped with small amounts of Ba shows that the line shapes are almost identical to those for sample *C*.

The Cu $2p_{3/2}$ emission has been discussed in detail by Sawatsy and co-workers[28] for a number of divalent Cu systems. They demonstrated that the main line is due to ligand screening of the $2p$ core hole via the final-state configuration $2p_{3/2}d^{10}\underline{L}$ where the underbar denotes a hole and L describes a suitably symmetrized screening ligand p orbital. The broad doublet is composed of eight multiplet states which are the result of the interaction of the $2p_{3/2}$ hole with the d^9 valence electrons in the final state. Their work suggested that the relatively large width of these core-level features reflects mixing of the two photoemission final states. Fujimori *et al.*[15] and Shen *et al.*[16] extended this discussion to the Cu-O-based superconductors. Using the satellite-to-main-line intensity ratio and the peak energy separation, they calculated the ground-state d-electron occupation number, the Cu-O charge-transfer energy, the d-d Coulomb interaction ($\sim$6 eV), and the ligand-d hybridization energy. Their results clearly showed the importance of photoemission final-state effects for these Cu-O based materials. At the same time, it should be clear from Fig. 1 that the experimental parameters depend on the quality of the surface studied. Steiner *et al.*[17] provided detailed discussions of the Cu line shape for a variety of Cu-O systems, showing the $2p$ core-level spectra for formally 1^+, 2^+, and 3^+ valent compounds. They, and others, have sought to define the formal valence of Cu, and all of the spectroscopic results indicate that the valence of Cu is 2^+ in the 1:2:3 and 2:1:4 superconductors. At the same time, none of the photoemission results have revealed differences which might indicate inequivalent Cu sites in the lattice, either because of inherent final-state effects noted above or because, as suggested by the calculations of Herman, Kasowksi, and Hsu,[24] the charge within the Cu site is very nearly the same for all Cu atoms. (We shall return to the topic of Cu valence in discussions of Cu adatom interactions.)

At the top right-hand side of Fig. 1 we show EDC's for the Y $3d_{3/2,5/2}$ core levels. Comparisons indicate that the spin-orbit splitting is best resolved for sample *C* because the results for samples *A* and *B* exhibit a high-binding-energy tail and a filling in of the minimum between the spin-orbit-split doublet. These differences indicate that a second bonding configuration for Y exists for samples *A* and *B*, probably a form of Y oxide. Analogous broadening is seen in the shallow Y $4p_{1/2,3/2}$ core levels, as indicated at the bottom of Fig. 1.

Finally, at the bottom of Fig. 1 we show the valence-band emission within 35 eV of E_F for samples *B* and *C*. The results for sample *B* are very similar to those in the literature, showing complex Ba $5p$ emission near 15 eV, poorly resolved Y $4p$ emission near 24 eV, and Cu-O hybrid states near E_F dominated by emission at $\sim$5 eV. The results for sample *C* are strikingly different, as might have been expected based on the core-level emission. In particular, the Y $4p_{1/2,3/2}$ doublet is better resolved and the high-binding-energy Ba $5p$ contribution has vanished (as it did for the Ba $3d$ emission) leaving a single spin-orbit-split doublet (binding energies of 12.5 and 14.2 eV). Significantly, the Cu-O hybrid states are also much better resolved, the emission centroid for sample *C* is shifted toward E_F relative to that for *A* or *B*, the central maximum appears at 3 eV, and there is a distinct shoulder at 1.8 eV. Most other experimental studies of the valence-band features of $YBa_2Cu_3O_{7-x}$ have reported Cu-O hybrid states within $\sim$8 eV of E_F and a very low density of states at E_F. As shown by Fig. 1, these conclusions still hold for clean $YBa_2Cu_3O_{6.9}$, with corrections to account for distortions due to the second phase. In many of the spectra in the literature, these distortions are very severe, with relatively little contribution from the superconductor itself. In particular, the structure at 3 eV which dominates the EDC's for the clean surface has been obscured by strong emission from Ba-O features. (Further discussion of the valence-band structure is found in the following section.)

To summarize, the results for sample *C* reveal the spectral features of the clean high-T_c superconductor. Comparison with $La_{1.85}Sr_{0.15}CuO_4$ makes it possible to focus on the common features of these two classes of related superconductors. Interestingly, although our results for samples *A* and *B* indicate large emission from contamination, x-ray analysis of the samples shows single-phase behavior. This suggests that the volume fraction of the contaminant is quite small. Instead, the spectral contribution from contamination reflects the fact that samples fracture both transgranularly and along the contamination-bearing

grain boundaries—boundaries which, in turn, frustrate efforts to achieve high critical currents. The relatively small amount of (volume) contamination exposed at these internal surfaces distorts the photoemisson results because of the inherently high surface sensitivity of photoemission. Such distortions become greater as the mean free path diminishes, as has been seen in our synchrotron radiation photoemission studies through the Ba $5p$ emission.

A picture of the exposed surface with suitable chemical and spatial resolution would reveal portions of the clean superconductor exposed by fracture, together with varying amounts of the grain boundary or intergranular phase(s) coating grains of superconductor. On a different scale, it would also show voids that account for deviations from 100% density. Our results show that the amount of the grain-boundary phase varies with sample preparaton: It was very small for sample C and for $La_{1.85}Sr_{0.15}CuO_4$, but was much larger for samples A and B. Unfortunately, it is impossible to estimate the amount of this grain-boundary phase because of the complex morphology of the surface.[31]

B. Experimental valence bands and band calculations for $YBa_2Cu_3O_{6.9}$ and $La_{1.85}Sr_{0.15}CuO_4$

In the two panels of Fig. 2 we compare our photoemission and inverse photoemission results for sample C of $YBa_2Cu_3O_{6.9}$ to analogous results for $La_{1.85}Sr_{0.15}CuO_4$. Also shown is a direct superposition of our XPS valence-band spectra for these two superconductors to draw attention to their similarities. For this comparison, we have shifted E_F for the 1:2:3 compound 0.3 eV relative to that for the 2:1:4 compound, as indicated by the arrows. The dominant manifold of Cu-O hybrid states is virtually identical, with the exception of the maximum at 3 eV which is more pronounced for $YBa_2Cu_3O_{6.9}$. Both exhibit three distinct valence-band features, a centroid at about -4 eV, a very low emission at E_F, weak emission to ~ 2 eV above E_F, and then strong empty-state emission. The origin of these empty-state structures is indicated. For $YBa_2Cu_3O_{6.9}$, the empty Ba $4f$ feature appears and the features closer to E_F represent Ba $5d$ and Y $4d$ bands. For $La_{1.85}Sr_{0.15}CuO_4$, the La $4f$ emission dominates for this incident electron energy, but the La $5d$ emission is also clearly evident. (See Ref. 19 for a complete discussion of the empty-state spectra.)

It is interesting to note that the band calculations for these two superconductors show greater differences than the experimental results would suggest.[22–27] Changes at E_F should be expected because the calculations show the crossing of three bands for the 1:2:3 material compared to only one for the 2:1:4. Beyond that, however, the band calculations for the 1:2:3 material predict a well-defined minimum between two prominent Cu-O derived structures (the resonance gap at M in the Brillouin zone). Those for the 2:1:4 predict no such minimum. These general observations can be seen from Fig. 2, where the calculated densities of states are reproduced. Mattheiss[22] and Hamann and Mattheiss[22] have treated both systems, predicting states extending from $+2$ to -5.5 eV for the 1:2:3 compound, with a centroid at about -2 eV and a bifur-

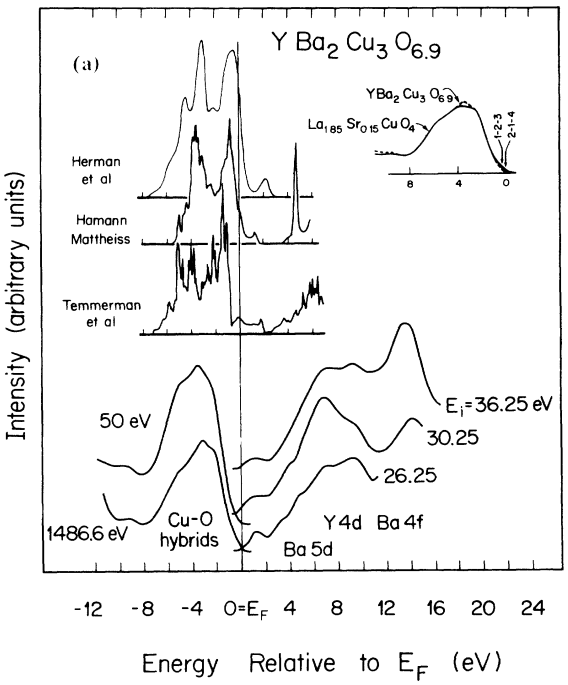

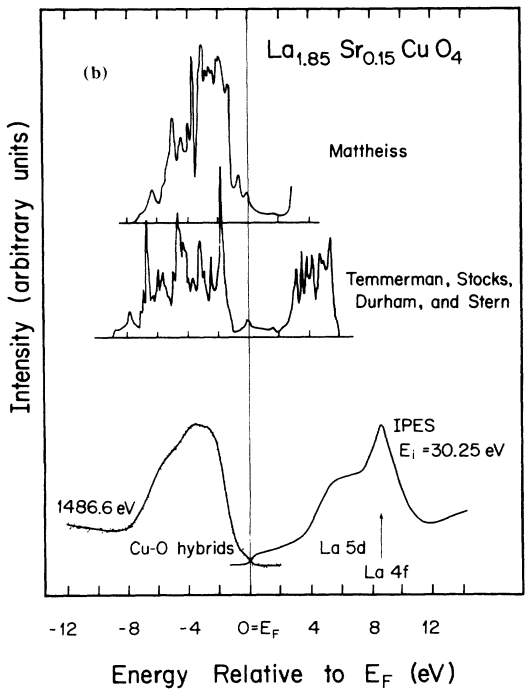

FIG. 2. Photoemission and inverse photoemission spectra for clean $YBa_2Cu_3O_{6.9}$ and $La_{1.85}Sr_{0.15}CuO_4$ showing the occupied states and empty states. The spectral features reflect Cu-O hybrids from approximately -7 eV to -2 eV for both superconductors, together with the empty La $5d$, Ba $5d$, Y $4d$ bands, and the atomiclike La and Ba $4f$ states (see Ref. 19 for a detailed discussion). Calculated densities of states are shown above the experimental spectra, as discussed in the text. Direct superposition of the experimental results for the 1:2:3 and 2:1:4 compounds shows their compelling similarity.

cated structure around this centroid. For the 2:1:4 compound, the predictions show the centroid at approximately -3 eV and the bifurcation to be missing. In neither case is there strong emission from the vicinity of the Fermi level. Comparison to the XPS results suggests that the experimental centroid lies approximately 1 eV deeper than these authors predict for both compounds.

In Fig. 2 we have also reproduced the density of states from Temmerman *et al.*,[25] who considered both materials, and Herman, Kosowski, and Hsu,[24] who examined the effects of oxygen stoichiometry for $YBa_2Cu_3O_x$. For the 2:1:4 compound, the calculations by Temmerman *et al.* predict a broader Cu-O manifold and a centroid which is slightly deeper than that observed experimentally. For $YBa_2Cu_3O_{6.9}$, they also predict a bifurcated structure, but it is less severe than that in the calculations of Hamann and Mattheiss or Hermann and co-workers. Again, their Cu-O centroid is the deepest of the three, and all are 1–2 eV closer to E_F than we see in the XPS spectra.

This shift in the centroid has been used to argue for strong hole-hole repulsion at the Cu sites, consistent with correlation effects observed in the core-level and valence-band satellite structures noted above.[15,16,23] (Unfortunately, several of the early experimental papers were troubled by contamination which shifted the centroid to even greater binding energy, as can be seen from Fig. 1 or Ref. 18.) Redinger *et al.*[23] calculated the photoemission spectra for La_2CuO_4-derived materials and Fujimori *et al.*[15] corrected their experimental EDC's to try to account for photoionization cross-section variations. Comparison of the predicted and experimental results, as shown in Fig. 2, showed poor agreement. Subsequent analysis led to suggestions that *d-d* Coulomb correlation effects would shift the experimental Cu-derived structures 1.5–2 eV to greater apparent binding energy. Less significant shifts would be expected for states of predominantly oxygen $2p$ character. Account of these final-state effects would substantially improve agreement between experiment and at least some of the calculated one-electron densities of states. They would not, however, eliminate the theory-to-theory variation.

Comparison of these XPS results for the valence band to lower photon energy EDC's taken with synchrotron radiation shows that the experimental features have very little $h\nu$ dependence (see spectra in Fig. 2 for $h\nu=1486.6$ and 50 eV, with the caveat that our Ba $5p$ core-level results for $h\nu=50$ eV showed more broadening than did the XPS spectra, and it is likely that the emission near 6 eV is stronger than it should be). This is in contrast to the calculated EDC's for La_2CuO_4 by Redinger *et al.*[23]

It is apparent that if more valence information is to be extracted from photoemission, it should be sought through angle-resolved studies. Unfortunately, the preliminary results of Stoffel *et al.*[9] for single crystals of $YBa_2Cu_3O_x$ showed relatively little new structure, no doubt because of the multiplicity of Cu-O hybrid bands that contribute to the dominant valence-band features. Their results do, however, show subtle changes near the Fermi level which indicate dispersion of the uppermost bands. Similar dispersive changes near E_F can be observed through the inverse photoemission spectra shown in Fig. 2. In particular, the intensity and shape of the Cu-O emission near E_F is seen to change with incident electron energy. Furthermore, an angle-integrated bremsstrahlung isochromat spectrum at $h\nu=1486.6$ eV clearly displays a sharp minimum at ~ 2 eV above E_F, in good agreement with calculations for the top of the Cu-O antibonding band. Unfortunately, the polycrystalline nature of our samples has so far prevented empty-state band mapping.

Finally, it should be noted that there is a weak feature for $YBa_2Cu_3O_{6.9}$ at 9.4 eV. The intensity of this feature varies in the different EDC's in the literature, but it has consistently been observed. Part of it in the early studies may be related to C $2s$ emission, but even those studies (such as ours here) which examined samples that were carbon free found it to be present. To our knowledge, a definitive explanation for the 9.4-eV feature is still not available. Its presence in 1:2:3 and 2:1:4 compounds which are carbon free and have only Cu and O in common points to one of these as the source.[31]

C. Surface modifications by argon sputtering

In this section we discuss changes observed when fractured surfaces of $YBa_2Cu_3O_{6.9}$ were exposed to argon ion bombardment. Part of the motivation for this study was that Ar^+ sputtering is routinely used to prepare clean surfaces for study—and it had been reported that air-exposed high-T_c surfaces could be sputtered clean prior to metallization. Our results show, however, that sputtering leads to the disruption of the surface region and the likely loss of superconductivity. For polycrystalline, air-exposed surfaces it leads to atomic redistributions and unknown final configurations. Moreover, these depend on the starting surface and the sputtering conditions.

Cursory examination of the results for 500-eV sputtering shows that the O $1s$ emission always decreases with sputtering time. For sample *C*, the total O emission decrease was 10% over the first ten sputter cycles (each of 30-s duration), then decreased only slightly during 2 h of subsequent sputtering. At the same time, there was a continuous shift to higher binding energy of the O $1s$ emission. This shift, which amounted to $+0.6$ eV during 2 h of sputtering, indicated a change in environment for oxygen as the bonding configuration characteristic of the superconductor was lost. The fact that the oxygen emission changed during early sputtering probably reflects atomic redistribution within the probed region. The O $1s$ stability thereafter suggests that the amount of oxygen did not change dramatically. Although one must be cautious in interpreting these results because of preferential sputtering, they fail to give any indication of massive oxygen depletion in the surface region. Likewise, none of our other results indicated the loss of oxygen from fractured or sputtered surfaces due to inherent instabilities.

Sputtering of sample *A* revealed analogous trends for the superconductor-related oxygen emission. However, sputtering of the partially contaminated surface also led to a rapid drop in total oxygen emission because of rapid modification of the contaminant phase at the surface. Indeed, for sample *A* there was a 40% drop in O emission during the first hour of sputtering. We conclude that

sputtering reduced grain-boundary contamination, though it also disrupted the superconductor.

Equally dramatic Ar^+-induced changes were observed in the Ba $3d_{5/2}$ and Cu $2p_{3/2}$ core-level EDC's. For the partially contaminated samples, there was a change in relative intensity of the two Ba $3d$ components as the superconductor environment was lost and one that was more like that of the contaminant was formed. For the cleaner $YBa_2Cu_3O_{6.9}$, it was possible to see an overall $3d$ shift in binding energy as the superconductor environment was destroyed. For Cu, the $2p_{3/2}$ core-level EDC's showed a rapid loss of the satellite intensity, signaling a change from a nominally divalent to a nominally monovalent state. This loss was observed for both clean and partially contaminated $YBa_2Cu_3O_{6.9}$ with a faster conversion rate for the clean surface, presumably because it was less protected by a grain-boundary-phase skin. These rapid changes indicate the destructive effects of even low-energy Ar^+ bombardment; although sputtering removes the second phase, it also suppresses superconductivity in the probed region (depth at least 30 Å).

1. *Ti/$YBa_2Cu_3O_{6.9}$ interface formation*

The results discussed above show that the surfaces of these high-temperature superconductors are complicated and are readily modified by Ar^+ ion bombardment or exposure to atmospheric gases. In this section and the next, we examine the stability of these surfaces when exposed to adatoms of Ti and Cu. As we will see, both induce profound changes in the near-surface region and complex, metastable interfaces evolve.

In Fig. 3 we show a representative collection of Ti $2p$ core-level EDC's measured following the deposition of Ti onto sample *C*, starting with 0.5 Å (bottom) and proceeding through 48 Å (top). These spectra are normalized to constant peak height. These results highlight the changes in chemical state of the adatoms as the interface evolved. At lowest coverage, the $2p_{3/2}$ structure is very sharp while that for the $2p_{1/2}$ core is much broader, as is observed in a range of Ti-O systems.[31] With increasing deposition, these Ti features shift rigidly to *higher* binding energy, with slight changes in line shape. After 4 Å the Ti $2p_{3/2}$ structure is clearly distorted and is shifted 1.2 eV relative to its position at lowest coverage. This shift to higher binding energy indicates that the oxidation state has evolved as the amount of Ti has increased. (As will be discussed below, this evolution is associated with the progressive loss of oxygen from the substrate.) The fully reacted product observed at 4 Å is most likely TiO_2-like in bonding configuraton,[32] though these interface reaction products are spatially constrained and are not likely to develop extended crystallites. Moreover, the results for 4 Å show a second Ti chemical configuration that appears at $\sim$2 eV *lower* binding energy. This new component grows with coverage and ultimately dominates the EDC by $\sim$8 Å. Inspection of Fig. 2 shows that it shifts to lower binding energy until it reaches a final position at 453.8 eV (spin-orbit splitting 6.3 eV). This final configuration reveals the growth of a metallic Ti overlayer, the shift in binding energy and reduction in full width at half maximum indicating convergence to Ti metal. The final line shape indicates metallic screening of the core hole.[33] At the same time, its energy and width when first observed suggests that the progression from the TiO_2-like configuration seen at 4 Å to Ti metal is gradual as oxygen diffuses into the Ti layer and forms metal-rich Ti—O bonding configurations. We note that the attenuation behavior of the substrate core-level emission is quite complex. Significantly, if the attenuation rates for O $1s$, Cu $2p_{3/2}$, Ba $3d_{5/2}$, and Y $3d$ are compared, we find that oxygen is attenuated at a slower rate than Y, whereas from the photoelectron mean free paths we would have expected the opposite. This is consistent with oxygen out diffusion into the growing reacted Ti overlayer. The at-

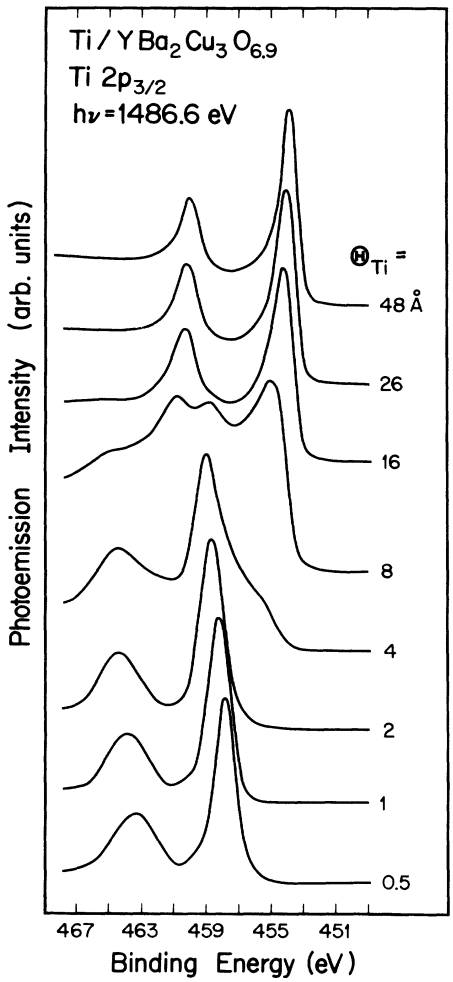

FIG. 3. Core-level EDC's for Ti $2p_{1/2,3/2}$ as a function of Ti deposition onto sample *C*, The spectra, which are normalized for visual clarity, show the increased oxidization state of Ti for coverages below $\sim$4 Å. At intermediate coverages (4–16 Å), our measurements detect both fully oxidized Ti-O and a new component which shifts with coverage as the O coordination by Ti increases. For coverages greater than 16 Å, the results show metallic Ti. These results indicate a metasable interface limited in extent by diffusion of oxygen to sites where adatoms of Ti arrive.

tenuation rates for all of the substrate constituents are much slower than would be found for a layer-by-layer growth mode. From these results, it is clear that the interface reaction products and morphology are complex.

It is important to note that the growth of the Ti overlayer on $La_{1.85}Sr_{0.15}CuO_4$ parallels that summarized in Fig. 3, although the spectral changes occur at slightly lower coverages for $La_{1.85}Sr_{0.15}CuO_4$ (Ref. 20). We conclude that the Ti-induced chemical modification of these two clean interfaces is very nearly the same. The coverage differences may reflect the slightly different morphologies for the starting surfaces. Significantly, the results of analogous experiments for partially contaminated $YBa_2Cu_3O_{6.9}$ surfaces of samples *A* and *B* are also very similar to those of Fig. 3, but the second component, corresponding to Ti metal, does not dominate until 16 Å (versus 8 Å for sample *C*). We suspect that this slower convergence to metallic Ti is a consequence of Ti adatom reaction with oxygen present in the grain-boundary phases. The eventual growth of metallic Ti is a consequence of kinetic limitations for O transfer to the surface, but the complex morphologies for these surfaces preclude quantitative modeling of these processes.

In Fig. 4 we summarize the behavior of the O 1*s* core-level EDC's during Ti deposition onto sample *C*. At low coverage, ≤ 1 Å, the dominant O 1*s* feature broadens and shifts to higher binding energy. This broadening reflects Ti—O bonding at the surface as well as modification of the bonding configurations for O that remains in the substrate. Moreover, the oxygen emission characteristic of the unchanged substrate also decreases. Line-shape decomposition makes it possible to quantitatively follow this rate at which emission from O atoms in the unaffected superconductor is attenuated. The substrate emission is reduced to 10% of its original intensity for a Ti coverage of 8 Å, suggesting major disruption at the interface for low coverages. At higher coverages when TiO_2 and the early metal-rich oxide form ($\Theta < 16$ Å), the dominant O 1*s* emission is centered at 530.5 eV. In turn, emission from this intermediate bonding form of O is attenuated when the final stage of interface formation starts, as can be seen from the EDC at 26 Å. This suggests a sequence of bonding configurations for O with one growing over the other rather than at its expense. Comparison of the O 1*s* results for sample *C* to those for $La_{1.85}Sr_{0.15}CuO_4$ shows parallel behavior because of analogous process involving reaction with Ti.[20] However, for Ti overlayer growth on samples *A* and *B* of $YBa_2Cu_3O_{6.9}$, the O 1*s* emission for the clean surface persisted to higher coverages (28 Å), but the O evolution was more difficult to observe because the O 1*s* was much more complex for the starting surface (see Fig. 1).

In Fig. 5, we show the Ti-induced changes in the Ba $3d_{5/2}$ core-level emission for sample *C*. For Ti depositions up to 8 Å, there is a steady loss of intensity from the feature at 778.3 eV and the growth of a new feature at higher binding energy as the overall $3d_{5/2}$ emission broadens. As for the O 1*s* emission, these results clearly show Ti-induced changes in bonding configurations. They offer information that could not be obtained from the O spectra, however, because the Ba atoms are less mobile

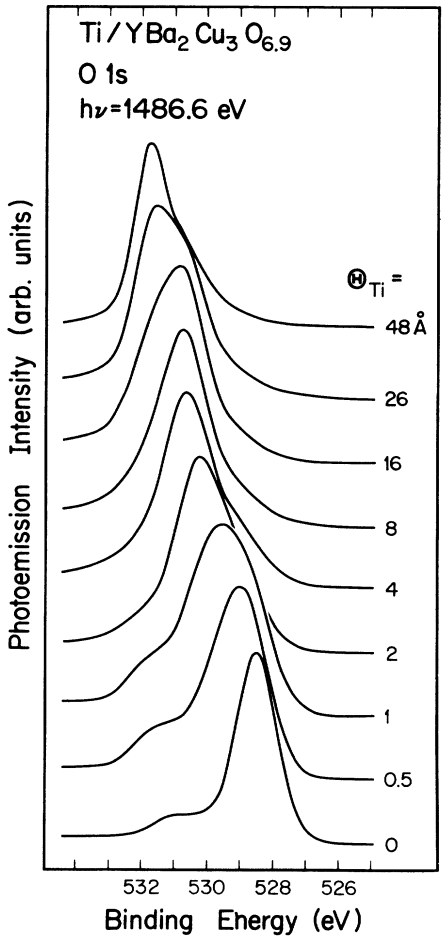

FIG. 4. O 1*s* core-level EDC's as a function of Ti deposition. Changes at low coverage indicate the Ti-induced modification of the O bonding. The feature at ~530 eV is related to the growth of TiO_2. At highest coverage, the O 1*s* emission reflects oxygen in solution in Ti.

than O and more directly sample the changing superconductor. These changes therefore represent modification of the superconductor that is a consequence of the loss of oxygen. (Again, we should note that the EDC's in this paper are normalized to emphasize changes in line shape rather than reflect absolute emission intensities. In an absolute sense, the deposition of 8 Å of Ti reduces the total Ba $3d_{5/2}$ emission to 37% of its initial value while line-shape decomposition shows the very rapid loss of the chemical configuration representative of the superconductor. Analogous results for the Ba $3d_{5/2}$ core-level evolution of Ti overlayers on partially contaminated $YBa_2Cu_3O_{6.9}$ surfaces show a complex line shape for the depositions between 1 and 16 Å. This is due to overlap in emission of the Ti-induced reaction product (as in Fig. 5) and the impurity emission present for the starting surface (Fig. 1).

In Fig. 6, we show the Cu $2p_{3/2}$ core-level emission as a function of Ti coverage. The most striking result is that very little Ti leads to the complete loss of the Cu^{2+} satel-

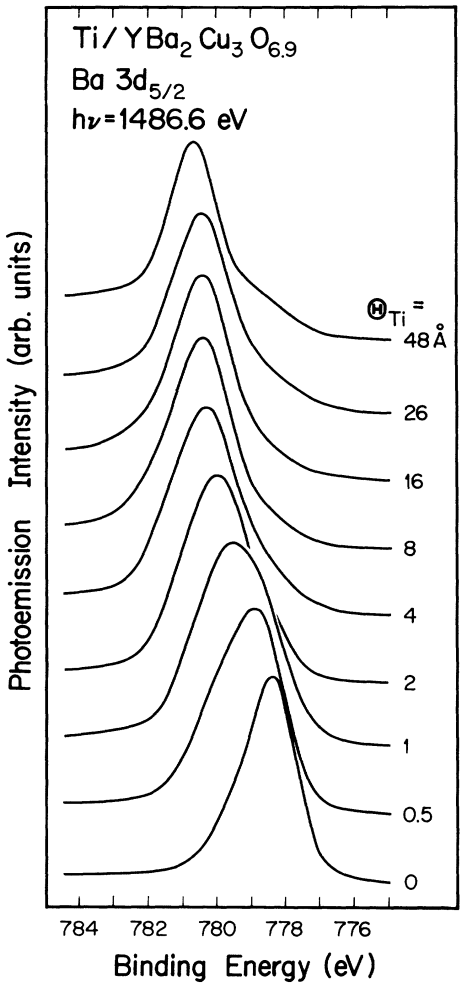

FIG. 5. Ba $3d_{5/2}$ core-level EDC's as a function of Ti deposition where the feature for the clean surface is attributed to the superconducting phase and the shift to higher binding energy reflects changes in the superconductor matrix induced by the loss of oxygen and its reactions with Ti.

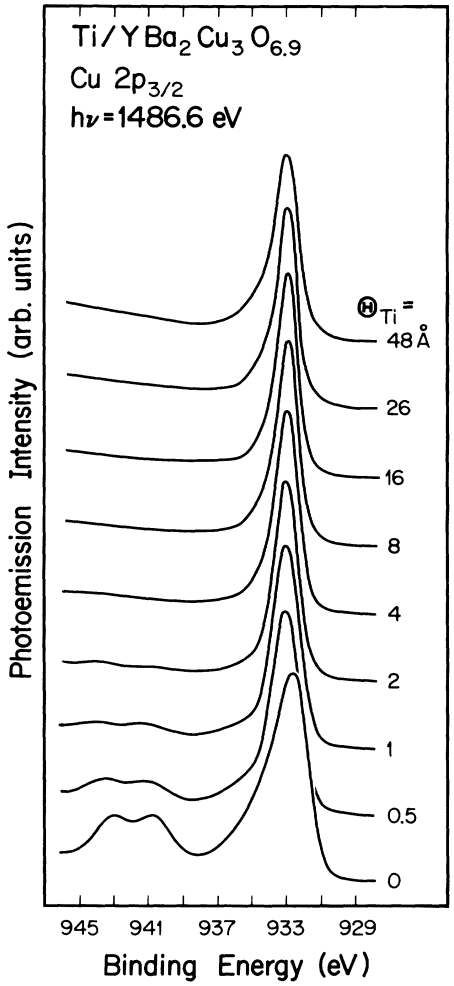

FIG. 6. Cu$2p_{3/2}$ core-level EDC's as a function of Ti coverage showing the main line and the envelope of satellites, as discussed in the text. As adatoms of Ti react with oxygen withdrawn from the substrate, the emission from Cu^{2+} satellites is attenuated and the main peak sharpens, reflecting reduction to a nominal Cu^{1+} configuration within the volume probed by photoemission (30–50 Å depth).

lite emission within the probe depth of our experiments (30–50 Å at these energies since the mean free path of the photoelectron is ~5 Å and there is a spread about the 60° emission angle relative to the surface normal because of the fractured character of these surfaces). Even the deposition of 0.5 Å results in the sharpening of the main line and the reduction of the total satellite emission by ~50%, and 1 Å reduces the satellite to 25% of its initial emission. As noted above, 1 Å of Ti corresponds to the equivalent of ~0.28 monolayers based on the atom density of the Cu-O planes. At these ultralow coverages, the attenuation of the substrate signal by the adatoms is negligible, implying that the volume of material probed has not changed appreciably from that for the clean surface. The Ti-induced changes in the Cu $2p_{3/2}$ emission show the fragile nature of the Cu^{2+} bonding configuration for these superconductors.

These results for the Cu core level go significantly beyond what could have been concluded based only on the fact that oxygen was lost and that Ti-O formed at the surface. Indeed, the loss of a small amount of oxygen might have been expected because it is possible to convert the semiconducting phase to a superconducting phase by suitable charging with oxygen (increase of oxygen content from 6.5 to 6.9 atoms per formula unit). However, during these changes the Cu-O planar structures do not change and Cu^{2+} bonding configuration is stable. Instead, what is surprising is that the adatom-induced changes completely suppress the Cu^{2+} configuration within the volume sampled by our measurements—this cannot be explained by a simple outdiffusion of oxygen from an unmodified $YBa_2Cu_3O_x$ structure. Rather, it reveals a surprisingly long-range structural destruction. Moreover, these Cu results are consistent with those for Ba where a few angstroms of metal produced new bonding configurations throughout the probed region. Finally, analogous effects were observed for Ti overlayers deposited onto clean $La_{1.85}Sr_{0.15}CuO_4$ where there are no Cu-O chains.[20] The

absence of the Cu-O chains in $La_{1.85}Sr_{0.15}CuO_4$, but the compellingly similar Cu $2p$ behavior, indicates that oxygen is also leached from the Cu-O planes for both systems.

In Fig. 7 we show Ti-induced changes in the valence bands and shallow core levels for sample *C*. For Ti depositions below 4 Å, the emission near E_F decreases, consistent with oxygen loss and structural modification of the probed region. This is analogous to what we have observed with other reactive interfaces (adatoms of Fe, Al, Pd, La, and Ge). Changes near E_F can best be seen through difference curves of the sort shown in Ref. 20. Hence, the newly-formed region is likely to be poorly conducting, at best. When the amount of deposited Ti reaches 8 Å, the emission at E_F increases as Ti metal nucleates. From Fig. 3, metallic Ti $2p$ emission also appears at this coverage. These valence bands also show structure near 7 eV which appears at ~8 Å and persists to the upper limit of our measurements. We associated this with

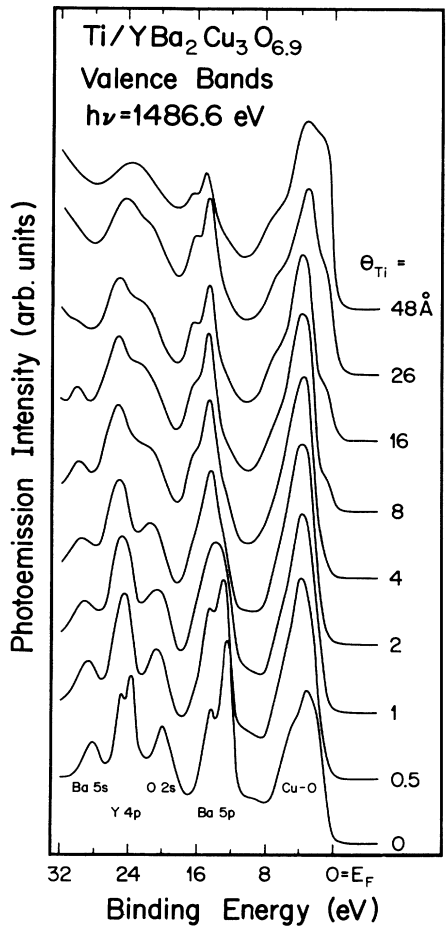

FIG. 7. Valence band and shallow core-level emission for clean and Ti-reacted $YBa_2Cu_3O_{6.9}$. Titanium deposition below 4 Å depletes states within 1 eV of E_F; at intermediate and higher coverages there is increased emission at E_F due to the nucleation and growth of Ti metal. The structure near 7 eV reveals a Ti-rich configuration for O in a metal matrix. The Ba $5p$, Y $4p$, and O $2s$ emission shows the appearance of multiple chemical configurations related to structural disruption of the superconductor.

O in solution in the Ti-rich overlayer, by analogy to what is observed from the O $1s$ emission and the measurements of others for Ti oxidation.[34] From Fig. 7, we can see that the O $2s$ emission also persists, shifting to higher binding energy and being partially responsible for the broad feature at ~24 eV at 48 Å. At higher coverages, the Ti d-band emission near the Fermi level grows as the surface region converges to Ti. Analgous behavior is observed for Ti deposition on $La_{1.85}Sr_{0.15}CuO_4$. In that case, the oxygen emission is ultimately lost because the measurements extended to 100-Å deposition.

The results of Fig. 7 provide evidence that the Ba bonding configuration changes during interface evolution, supporting conclusions based on deeper core levels. As shown, the well-resolved Ba $5p_{1/2,3/2}$ doublet at 12.5 and 14.2 eV is badly distorted by the deposition of 1 Å of Ti. The Ba $5p$ line shape sharpens above 1 Å as the probed region converges to the new, no-longer-superconducting bonding configuration with a Ba chemical shift of ~1.5 eV to higher binding energy, again corresponding to what was shown in Fig. 5.

Finally, in the high-coverage spectra for these core levels, there is weak emission in binding energies which correspond to those of the substrate, together with stronger emission from chemically shifted states. This reflects small regions which have not been covered up by the adatoms. It can be understood in terms of the complex morphology of the fractured surface and shadowing effects for a rough surface. Quantitatively, the total Y $3d$, Ba $3d$, and Cu $2p$ emission reduced to 3% of the original emission by 48-Å deposition.

2. *Cu/$YBa_2Cu_3O_{6.9}$ interface formation*

To further examine the stability of the superconductor against oxygen loss and structural degradation, we investigated Cu adatom interactions with the clean 1:2:3 surface. In Fig. 8 we show EDC's for the O $1s$ core level for Cu depositions between 0.5 and 46 Å. For this fracture, the amount of second phase was greater than that of Fig. 1. The deposition of Cu leads to a broadening and shift towards higher binding energy of the dominant O $1s$ emission feature (0.3 eV full-width-at-half-maximum increase and total shift of 0.75 eV within the first 4 Å, with negligible changes thereafter). The binding-energy shift implies that the effect of Cu adatoms is very similar to that of Ti, although to a lesser extent. In contrast, the feature associated with the impurity phase is unaffected by the deposition of Cu and does not shift or broaden measurably. This indicates preferential reaction of Cu adatoms with the high-T_c phase. Quantitative assessments of the rate at which the total O $1s$ emission intensity is attenuated show that it persists more than would have been expected for layer-by-layer overlayer growth on a smooth surface (~12% of the clean-surface value after 86-Å Cu deposition). This is a consequence of O outdiffusion and reaction with Cu and a nonplanar starting surface. This outdiffusion is also reflected by the changing intensity ratio of the two O $1s$ features since the superconductor phase contributed ~75% of the total O $1s$ intensity for the clean surface, but the contribution of the reaction-

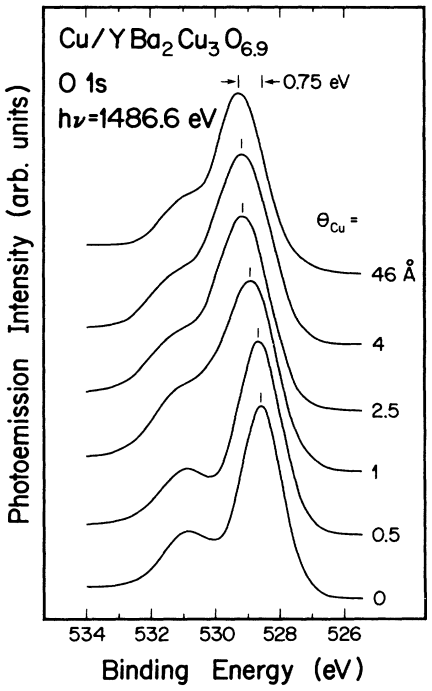

FIG. 8. O 1*s* core-level EDC's for Cu deposition onto $YBa_2Cu_3O_{6.9}$ as in Fig. 4 for Ti adatoms.

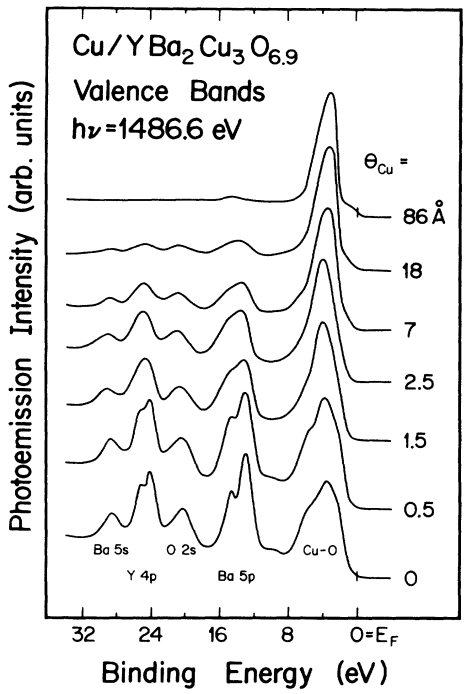

FIG. 9. Valence bands and shallow core levels of $YBa_2Cu_3O_{6.9}$ as a function of Cu coverage, analogous to those of Fig. 7.

induced low-binding-energy feature increased to 85% by 26 Å of Cu coverage.

In Fig. 9 we show the Cu-induced changes in the valence bands and the shallow Y, Ba, and O core levels. As for Ti, the deposition of 0.5–2.5 Å of Cu reduces the emission at E_F because of disruption of Cu-O hybrids and structural modification. After 4 Å, the emission at E_F increases as Cu metal nucleates on the surface. These changes correlate well with the O 1*s* core-level shifts and indicate that surface reactions became kinetically limited at ~4-Å Cu deposition. (Note that this observation is for a complex interface, not a layer-by-layer system, and that nucleation of Cu clusters at one site may produce metallic emission before reaction at another becomes kinetically limited; the 300-μm-diam x-ray beam averaged over a great many such inequivalences.)

For Cu coverages between 0.5 and 4 Å, our results show an asymmetric broadening and shift toward higher binding energy of the Y 4*p*, Ba 5*p*, and O 2*s* emission (Fig. 9), indicating the creation of new, unresolved reaction products. These features attenuate with coverage with Y and Ba disappearing more rapidly than O. Chemically shifted components also appear on the higher-binding-energy side of the Y 3*d* and the Ba $3d_{5/2}$ core levels during the first 4 Å of Cu deposition. However, for higher coverages it was the reacted component of Ba that persisted, while it was the unreacted component of the Y signal which was strongest. This suggests that a small amount of Ba, freed by Cu disruption of the superconductor, segregates to the surface region of the thickening Cu overlayer. (The total Y 3*d* signal is reduced to ~3% of its original value by 86-Å Cu coverage, while the total Ba $3d_{5/2}$ signal is reduced to only ~10% of its initial intensity. The Y emission can be understood because of shadowing, but if only shadowing were important then the emission 5f both Y and Ba should attenuate at the same rate.) Similar results have been found for synchrotron radiation studies[21] of $Cu/YBa_2Cu_3O_{6.9}$. This is in contrast with the results for the Ti overlayer, where it was seen that the emission from all species except oxygen attenuated the same.

Finally, in Fig. 10 we show representative Cu $2p_{3/2}$ EDC's which confirm surface reaction at low coverage and convergence to Cu metal at high coverage. On the left-hand side we show the region of the Cu satellites, enhanced to yield the same maximum value after subtraction of a flat background. The relative sizes of these features can be seen from the spectra on the right-hand side. As shown, the Cu^{2+} satellite features are attenuated almost as rapidly by Cu adatoms as by Ti adatoms. By 1.5 Å, the satellite structure is severely distorted as the feature at 944 eV dominates. Its presence and the loss of the strong 2^+ satellite emission indicates the conversion of Cu from 2^+ to 1^+, and the results on the right-hand side show a main line shift of only 0.3 eV, as shown on the right-hand side. Significantly, Cu adatom bonding, which induces changes in the superconductor surface at low coverage, exhibits the same Cu^{1+} configuration that is observed for the disrupted superconductor several angstroms into the matrix. (Spectroscopically, Cu at the surface is not distinguishable in core-level photoemission from that in the buried matrix, despite different atomic environments.) At higher coverage, the valence-band results indicate nucleation of Cu metal, and the Cu $2p_{3/2}$ results of Fig. 10 show a gradual shift in binding energy as the emis-

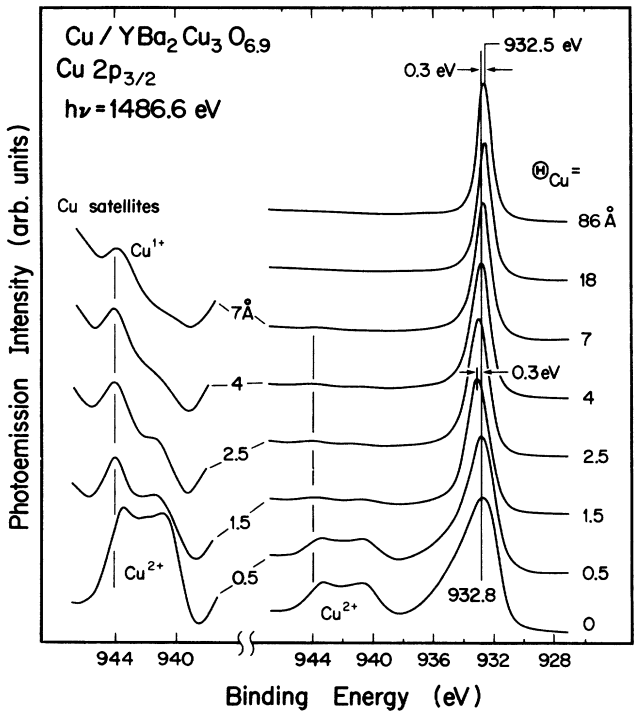

FIG. 10. Cu $2p_{3/2}$ EDC's for the $Cu/YBa_2Cu_3O_{6.9}$ interface showing rapid reduction of the superconductor Cu^{2+} configuration. As shown at the right, there is a shift of 0.3 eV to higher binding energy during the conversion from Cu^{2+}. The results on the left-hand side highlight the satellite feature; they were obtained by subtracting a constant background from the spectra on the right-hand side and scaling to give spectra with uniform height for visual but not quantitative inspection. As shown, by 1.5-Å deposition, the satellite structure shows the presence of the distinctive Cu^{1+} feature at 944 eV. This satellite persists as the Cu^{2+} satellite disappears. By 18 Å, the main line has shifted to 0.3 eV lower binding energy relative to the superconductor (932.5 eV), indicative of metallic Cu.

sion from Cu metal grows (final binding energy of Cu metal is 0.6 eV lower than for the disrupted Cu^{1+} matrix and 0.3 eV lower than for the clean superconductor). Comparison of recent synchrotron-radiation-photoemission results for samples of the *A* or *B* family shows similar evolution for the Cu valence-band satellites.[21] In particular, the resonantly enhanced d^8 final states for $YBa_2Cu_3O_{6.9}$ rapidly yield to the satellite structure of the d^9 final state and, ultimately, to the D^{10} satellites of Cu metal as the amount of deposited Cu increases.

Finally, comparison of these results for $Cu/YBa_2Cu_3O_{6.9}$ to those for $Cu/La_{1.85}Sr_{0.15}CuO_4$ (Ref. 20) shows analogous behavior for Cu in the superconductor, in the disrupted region, and in the final metal layer. The principal difference is that the onset of Cu metal formation began at slightly higher coverage for $YBa_2Cu_3O_{6.9}$ compared to $La_{1.85}Sr_{0.15}CuO_4$.

III. SUMMARY

In this paper we have compared valence-band and core-level photoemission spectra for a variety of samples of $YBa_2Cu_3O_{6.9}$, emphasizing results characteristic of the clean surface and comparing them with results for clean $La_{1.85}Sr_{0.15}CuO_4$. The present results show that the XPS valence-band spectra of $YBa_2Cu_3O_{6.9}$ and $La_{1.85}Sr_{0.15}CuO_4$ are remarkably similar, more so than would be expected based on the various band calculations. Studies involving Ar sputtering and reactive adatom deposition have shown the stability of the nearly contamination-free and partially contaminated surfaces. We conclude that the Cu-O based 1:2:3 and 2:1:4 superconductors degrade rapidly, both at the surface and for a substantial distance into the substrate, due to the removal of oxygen from the superconductor and related structural changes of the matrix. These results suggest that reactions are kinetically limited by the diffusion of oxygen to the surface because it eventually becomes possible to form clean-metal overlayers. These interfaces are almost certainly metastable. Results such as these show that metals with high heats of oxide formation lead to substrate disruption and heterogeneous reaction across the interface. Of the many metals and semiconductor overlayers studied to date, only Au forms overlayers which do not adversely affect the superconductor.

ACKNOWLEDGMENTS

The work at Minnesota was supported by the University of Minnesota, U.S. Defense Advanced Research Projects Agency, and the Office of Naval Research; that at Argonne National Laboratory was supported by the Department of Energy under Grant No. W-31-109-Eng-38. Stimulating discussions with N. G. Stoffel are gratefully acknowledged

[1]C. W. Chu, P. H. Hor, R. L. Meng, L. Gao, Z. J. Huang, and Y. Q. Wang, Phys. Rev. Lett. **58**, 405 (1987).

[2]For a review of electron spectroscopic results for $La_{1.85}Sr_{0.15}CuO_4$ and $YBa_2Cu_3O_{6.9}$, see *Thin Film Processing and Characterization of High-Temperature Superconductors,* Proceedings of the American Vacuum Society Special Conference on High Temperature Superconductivity, Anaheim, California, 1987, edited by. J. M. E. Harper, R. J. Colton, and L. C. Feldman, AIP Conf. Proc. No. 165 (American Institute of Physics, New York, 1988).

[3]P. Steiner, V. Kinsinger, I. Sander, B. Siegwart, S. Hüfner, and C. Politis, Z. Phys. B **67**, 19 (1987).

[4]P. D. Johnson, S. L. Piu, L. Jiang, M. W. Ruckman, M. Strongin, B. Sinkovic, N. V. Smith, R. J. Cava, C. S. Jee, D. Nichols, E. Kaczanowicz, R. E. Salomon, and J. E. Crow, Phys. Rev. B **35**, 8811 (1987).

[5]H. Ihara, M. Hirabayashi, N. Terada, Y. Kimura, K. Senzaki, M. Akimoto, K. Bushida, F. Kawadashima, and R. Uzuka, J. Appl. Phys. **26**, L460 (1987).

[6]J. A. Yarmoff, D. R. Clarke, W. Drube, U. O. Karlsson, A. Teleb-Ibrahimi, and F. J. Himpsel, Phys. Rev. B **36**, 3967 (1987).

[7]M. Onellion, Y. Chang, D. W. Niles, R. Joynt, G. Margaritondo, N. G. Stoffel, and J. M. Tarascon, Phys. Rev. B **36**, 819 (1987).

[8]R. L. Kurtz, R. L. Stockbauer, D. Mueller, A. Shih, L. E. Toth, M. Osofsky, and S. A. Wolf, Phys. Rev. B **36**, 8818 (1987).

[9]N. G. Stoffel, J. M. Tarascon, Y. Gang, M. Onellion, D. W. Niles, and G. Margaritondo, Phys. Rev. B **36**, 3986 (1987); N. G. Stoffel, Y. Chang, M. K. Kelly, L. Dottl, M. Onellion, P. A. Morris, W. A. Bonner, and G. Margaritondo, *ibid.* **37**, 7952 (1988).

[10]F. Garcia-Alvarado, E. Moran, M. Vallet, J. M. Genzalez-Calbet, M. A. Alavior, M. T. Perez-Frias, J. L. Vicent, S. Ferner, E. Garcia-Michel, and M. C. Asensio. Solid State Commun. **63**, 507 (1987).

[11]T. Takahasi, F. Mueda, H. Arui, H. Kutagama-Yoshida, Y. Okube, T. Suzuki, S. Hosoga, A. Fujimori, T. Shidata, T. Koide, T. Miyahara, M. Onoder, S. Shamato, and M. Soto, Phys. Rev. B **36**, 5686 (1987).

[12]N. Nücker, J. Fink, B. Renker, D. Ewert, G. Politis, J. W. P. Weigs, and J. C. Fuggle, Z. Phys. B **67**, 9 (1987).

[13]B. Reihl, T. Rieslerer, J. G. Bednorz, and K. A. Müller, Phys. Rev. B **35**, 8804 (1987).

[14]P. Steiner, J. Ablers, V. Kinsinger, I. Sander. B. Siegwart, S. Hüfner, and C. Politis, Z. Phys. B **66**, 275 (1987).

[15]A. Fujimori, E. Takayama-Muromachi, Y. Uchida, and B. Okai, Phys. Rev. B **35**, 8814 (1987).

[16]Z. Shen, J. W. Allen, J. J. Yeh, J. S. Kang, W. Ellis, W. Spicer, I. Lindau, M. B. Maple, Y. D. Dalichaouch, M. S. Torikachvili, J. Z. Sun, and T. H. Geballe, Phys. Rev. B **36**, 8414 (1987).

[17]P. Steiner, V. Kinsinger, I. Sander, B. Siegwart, S. Hufner, C. Politis, R. Hoppe, and H. P. Muller, Z. Phys. B **67**, 494 (1987).

[18]D. C. Miller, D. E. Fowler, C. R. Brundle, and W. Y. Lee, in Ref. 2, p. 336.

[19]H. M. Meyer III, Y. Gao, T. J. Wagener, D. M. Hill, J. H. Weaver, B. K. Flandermeyer, and D. W. Capone II, in Ref. 2, p. 254, Y. Gao, T. J. Wagener, J. H. Weaver, A. J. Arko, B. K. Flandermeyer, and D. W. Capone II, Phys. Rev. B **36**, 3971 (1987); **36**, 3899 (1987).

[20]D. M. Hill, H. M. Meyer III, J. H. Weaver, B. Flandermeyer, and D. W. Capone II, Phys. Rev. B **36**, 3979 (1987); D. M. Hill, Y. Gao, H. M. Meyer III, T. J. Wagener, J. H. Weaver, and D. W. Capone II, *ibid.* **37**, 511 (1988); H. M. Meyer III, D. M. Hill, S. G. Anderson, J. H. Weaver, and D. W. Capone II, Appl. Phys. Lett. **51**, 1750 (1987).

[21]H. M. Meyer III, D. M. Hill, S. G. Anderson, J. H. Weaver, and D. W. Capone, Appl. Phys. Lett. **51**, 1118 (1987); Y. Gao, T. J. Wagener, C. M. Aldao, I. M. Vitomirov, J. H. Weaver, and D. W. Capone II, J. Appl. Phys. (to be published); T. J. Wagener, Y. Gao, I. M. Vitomirov, J. J. Joyce, C. Capasso, J. H. Weaver, and D. W. Capone II, Phys. Rev. B **37**, 232 (1988).

[22]L. F. Mattheiss, Phys. Rev. Lett. **58**, 1028 (1987); L. F. Mattheiss and D. R. Hamann, Solid State Commun. **63**, 395 (1987).

[23]J. Redinger, J. Yu, A. J. Freeman, and P. Weinberger, Phys. Lett. A **124**, 463 (1987).

[24]F. Herman, R. V. Kasowski, and W. Y. Hsu, Phys. Rev. B **36**, 6904 (1987).

[25]W. M. Temmerman, G. M. Stocks, P. J. Durham, and P. A. Sterne, J. Phys. F **17**, L135 (1987).

[26]D. W. Bullett and W. G. Dawson, J. Phys. C **20**, L853 (1987).

[27]T. Fujiwara and Y. Hatsugai, J. Appl. Phys. **26**, L716 (1987).

[28]G. van der Laan, C. Westra, C. Haas, and G. A. Sawatsky, Phys. Rev. B **23**, 4369 (1981).

[29]S. A. Chambers, D. M. Hill, F. Xu, and J. H. Weaver, Phys. Rev. B **34**, 634 (1987); Y. Gao, M. Grioni, B. Smandek, J. H. Weaver, and T. Tyrie, J. Phys. E **21**, 489 (1988).

[30]J. D. Jorgenesen, H. B. Schuttler, D. G. Hinks, D. W. Capone II, K. Zhang, M. B. Brodsky, and D. J. Scalapino, Phys. Rev. Lett. **58**, 1024 (1987).

[31]Since this manuscript was submitted, we have completed high-resolution XPS studies of single crystals of the 1:2:3 and 2:1:4 materials that allow in-depth analysis of the oxygen 1*s* emission, confirmation of the intrinsic nature of the 9-eV feature, and more extensive comparisons for a broader base of materials. See J. H. Weaver, H. M. Meyer III, T. J. Wagener, D. M. Hill, Y. Gao, D. Peterson, Z. Fisk, and A. J. Arko, Phys. Rev. B **38**, 4668 (1988). Moreover, we have examined single-crystal $YBa_2Cu_3O_{7-x}$, where $x \sim 0.1$. By comparison to sample *C* in this paper, we know that x for sample *C* is less than 0.1. This does not alter any of our conclusions.

[32]G. Rocker and W. Gopel, Surf. Sci. **181**, 530 (1987).

[33]S. Doniach and M. Sunjic, J. Phys. C **3**, 285 (1970).

[34]D. M. Hanson, R. Stockbauer, and T. E. Madey, Phys. Rev. B **24**, 5513 (1981).